

 Open Access Full Text Article

ORIGINAL RESEARCH

Pre-Treatment with Zirconia Nanoparticles Reduces Inflammation Induced by the Pathogenic H5N1 Influenza Virus

This article was published in the following Dove Press journal:
International Journal of Nanomedicine

Caiyun Huo¹

Jin Xiao²

Kai Xiao¹

Shumei Zou³

Ming Wang^{1,2}

Peng Qi²

Tianlong Liu⁴

Yanxin Hu¹

¹Key Laboratory of Animal Epidemiology of Ministry of Agriculture, College of Veterinary Medicine, China Agricultural University, Beijing 100193, People's Republic of China; ²Key Laboratory of Veterinary Bioproduction and Chemical Medicine of the Ministry of Agriculture, Zhongmu Institutes of China Animal Husbandry Industry Co., Ltd, Beijing, People's Republic of China; ³National Institute for Viral Disease Control and Prevention, Collaboration Innovation Center for Diagnosis and Treatment of Infectious Diseases, Chinese Center for Disease Control and Prevention, Key Laboratory for Medical Virology, National Health and Family Planning Commission, Beijing, People's Republic of China;

⁴Laboratory of Veterinary Pathology and Public Health, College of Veterinary Medicine, China Agricultural University, Beijing 100193, People's Republic of China

⁴Laboratory of Veterinary Pathology and Public Health, College of Veterinary Medicine, China Agricultural University, Beijing 100193, People's Republic of China

Background: New approaches are urgently needed to fight influenza viral infection. Previous research has shown that zirconia nanoparticles can be used as anticancer materials, but their antiviral activity has not been reported. Here, we investigated the antiviral effect of zirconia (ZrO_2) nanoparticles (NPs) against a highly pathogenic avian influenza virus.

Materials and Methods: In this study, the antiviral effects of ZrO_2 on H5N1 virus were assessed in vivo, and the molecular mechanism responsible for this protection was investigated.

Results: Mice treated with 200 nm positively-charged NPs at a dose of 100 mg/kg showed higher survival rates and smaller reductions in weight. 200 nm ZrO_2 activated mature dendritic cells and initially promoted the expression of cytokines associated with the antiviral response and innate immunity. In the lungs of H5N1-infected mice, ZrO_2 treatment led to less pathological lung injury, significant reduction in influenza A virus replication, and overexpression of pro-inflammatory cytokines.

Conclusion: This antiviral study using zirconia NPs shows protection of mice against highly pathogenic avian influenza virus and suggests strong application potential for this method, introducing a new tool against a wide range of microbial infections.

Keywords: avian influenza virus, zirconia nanoparticles, cytokine storm, antiviral effect

Introduction

In recent years, a large number of rapidly-spreading viral outbreaks have placed considerable demands on healthcare infrastructure, sparking global concern.^{1,2} The emergence of severe acute respiratory syndrome coronavirus (SARS-CoV) in 2002,³ the H1N1 influenza pandemic in 2009,^{4–6} pandemics of the H5N1 and H5N7 strains of influenza A virus (IAV),⁷ and the devastating Ebola and Zika virus epidemics of 2014 and 2015 illustrate the severity of these outbreaks.^{8,9}

Among these viruses, avian influenza virus H5N1 has attracted a great deal of attention due to its rapid spread and high pathogenicity worldwide.^{10,11} The leading cause of death in infected patients is diffuse alveolar damage and hemorrhage in the lungs, which is caused by overactive inflammatory responses.^{12,13} Overproduction of inflammatory cytokines in H5N1-infected mice and humans, referred to as a cytokine storm, has been identified as the main cause of death associated with this virus.^{14,15} Vaccination remains the most effective preventive measure against influenza viruses. Nevertheless, vaccination effectiveness is decreasing as new variants arise through antigenic drifts or shifts.¹⁶ Although some antiviral drugs such as zanamivir (Relenza) and oseltamivir (Tamiflu) are currently in use, the

Correspondence: Yanxin Hu
Email 07033@cau.edu.cn

Tianlong Liu
Email liutianlong@cau.edu.cn

increasing emergence of drug-resistant strains affects their clinical application.^{17,18} Therefore, development of novel broad-spectrum prophylactic and therapeutic agents against IAV is urgently needed.

In recent decades, nanoparticles (NPs) have increasingly been applied as an inexpensive and easy-to-use detection method as well as a promising adjuvant against viral infections due to their unique physical and chemical characteristics and strong activation of the immune system. Due to these structural and chemical properties, nano-materials have several advantages over bulk materials of the same composition, including small size, high surface area-to-volume ratio, and ease of preparation and modification. NPs can affect immune responses by binding to serum proteins. In previous studies, NPs have shown specific immunomodulatory effects on immune cells, as well as antiviral, antioxidant, and anticancer capabilities.^{19–21} In particular, virus-like particles (alundum and mesoporous silica) have received great attention for potential application as adjuvants.^{22–24} However, because protein or DNA vaccines exhibit poor stability in vivo, most reported NPs have been used only as efficient antigen delivery systems. Although NPs can enhance immunity, few studies to date have focused on the antiviral function of NPs rather than using them only as protein or DNA carriers.²⁵ The nanomaterial-activated immune response must be overcome when NPs are used as carriers.^{26–28} To date, little attention has been paid to the antiviral effects of NPs without virus-based antigens. Nanoparticles of ZrO₂, a nano-sized and hollow colloidal metal oxide with controllable thickness, were synthesized using a robust sol-gel process and show superior catalytic activity for many reactions due to the unique physicochemical characteristics of the surface of ZrO₂.^{29,30} ZrO₂ has been widely used as a catalyst in many engineering applications and offers an environmentally-friendly option for chemical and pharmaceutical industries.³⁰ It is also used as an anticancer agent in the treatment of colon cancer.³¹ Despite their potential biomedical applications, few studies have reported on the use of ZrO₂ as an antiviral material.

In the present study, a series of NPs were investigated with regard to particle size, surface charge, and composition for NP-mediated protection of animals from highly pathogenic avian influenza virus H5N1 infection. The results showed that ZrO₂ with optimal physical and chemical characteristics could reduce mouse mortality, alleviate respiratory pathological changes, and inhibit viral replication in the lungs of H5N1-infected mice. Treatment with ZrO₂ prior to

influenza infection caused prompt initiation of the host antiviral response and alleviated the damage induced by cytokine storms during H5N1 infection. This is the first report of an in vivo antiviral effect of ZrO₂ against H5N1 infection, and provides a comprehensive and low-cost method for the protection of humans or animals against various viral infections.

Materials and Methods

Animals

Six–Seven-weeks-old female BALB/c mice were purchased from Vital River Laboratories (Beijing, China).

Preparation of NPs

SNs were prepared as previously described.³² Briefly, SNs were synthesized through a two-step selective-etching method. In the first step, organic–inorganic hybrid solid silica spheres (HSSSs) were elaborately designed with a three-layer sandwich structure. The core and outer layer, or shell, were made up of a pure silica framework hydrolyzed from tetraethylorthosilane (TEOS), and the middle layer comprised organic silica co-condensed from TEOS and N-[3-(trimethoxysilyl) propyl]ethylenediamine (TSD). In the second step, HSSSs were converted into SNs with an appropriate amount of aqueous hydrofluoric acid.

ZrO₂ was prepared as previously described.^{33,34} Briefly, SNs were employed as templates. SNs underwent a dewatering process prior to dispersal in a mixture of alcohol and acetonitrile. Ammonia was added to adjust the pH to a weakly alkaline value. The zirconium precursor was slowly injected into the mixture with magnetic stirring. The hydrolysis of zirconium was triggered in the weakly alkaline environment to induce the growth of small ZrO₂ using SNs as seeds. After 6 h of reaction, a ZrO₂ shell gradually formed on the surface of the SN seeds. The thickness of the shell can be controlled by adjusting the reaction time and the Zr:SN ratio. To remove the SN seed core, NaOH solution (1 mL, 1 M) was added, followed by reaction at 80°C for approximately 4 h. The ZrO₂ NPs thus obtained were collected through centrifugation and washed three times with deionized water.

Preparation of poly-styrene (PS) was prepared as previously described.³⁵ Briefly, 6 g of freshly distilled styrene (Merck), 250 mg of hexadecane, 5 mg of the fluorescent dye N-(2,6-diisopropylphenyl)-perylene-3,4-dicarbonimidamide, and 100 mg of the hydrophobic initiator 2,2'-azobis (2-methylbutyronitrile) were added to 24 g of water

containing 125 mg of the surfactant cetyltrimethylammonium chloride. After stirring 1 h for pre-emulsification, the miniemulsion was prepared by sonification for 120 s at 90% amplitude at 0°C to prevent polymerization. Polymerization was carried out at 72°C overnight. After the synthesis, surfactant was removed by Amicon ultrafiltration (100 kDa), extensive dialysis and washing. Before being used, the particle suspensions were dispersed by sonification.

The morphology and structure of NPs were observed with a JEOL-200CX transmission electron microscope. The average size and surface charge of the ZrO₂ NPs in 5% glucose were measured with a Zetasizer 3000HSA particle analyzer (Malvern Company, UK) at 25°C.

Intraperitoneal Administration and Viral Challenge

The nanomaterial or glucose was administered intraperitoneally to mice twice, one day apart. On the second day of administration, the viral challenge was given. The H5N1 influenza virus (A/chicken/Henan/1/2004) used in this study was isolated from infected chicken flocks. The 50% lethal dose (LD₅₀) was determined in mice following serial dilution of the stock in phosphate-buffered saline (PBS). The mice were anesthetized with Zoletil (Virbac, Carros, France) and infected with a dose of triple LD₅₀ by the intranasal route according to previously published methods.³⁶ Seven mice per group were used in the experiment over a period of 14 days. Body weights were determined every 2 days. Lung tissue samples were collected on days 3 and 6 post-infection. All experiments with the H5N1 virus were conducted in a biosafety level 3 containment laboratory. Animal experiments were approved by the Animal Ethics Committee of China Agricultural University (approval number 201206078) in accordance with the Regulations of Experimental Animals of Beijing Authority. Furthermore, all experimental protocols conformed to the guidelines of the Beijing Laboratory Animal Welfare and Ethics Committee and were approved by the Beijing Association for Science and Technology (approval number SYXK-2009-0423).

Histopathological and Immunohistochemical (IHC) Analyses

On days 3 and 6 post-infection, lung tissue samples from three mice per group were collected and fixed with 4% neutral formalin at room temperature for 48 h. Histopathological and viral antigen analyses of lung tissues on day 6 post-infection

were performed using hematoxylin and eosin (H&E) staining and IHC staining, as previously described.³⁷ Briefly, serial tissue sections were cut to 5-μm thickness after embedding in paraffin. Each slide was stained with H&E and examined using light microscopy (Olympus CX31). For IHC staining, sections were incubated in 10% normal goat serum in PBS for 30 min to block non-specific binding sites prior to reaction with the anti-influenza nucleoprotein mAb (AA5H, Abcam) at 1:400 dilution in PBS for 2 h. The slides were further incubated with goat anti-mouse IgG conjugated with avidin (Chemicon, USA) for 1 h, followed by incubation in biotinylated peroxidase (Victoria, BC, Canada) for an additional 1 h. Staining was visualized through the addition of 3,3-diaminobenzidin (Sigma-Aldrich, St. Louis, MO, USA) for 15 min and counterstaining with hematoxylin; the slides were then mounted with neutral balsam.

Pathological changes were evaluated by a veterinary pathologist and scored from 0 to 4 in a blind study. Descriptions of the lung scores were as follows: 0 = no microscopic lesions; 1 = extremely mild, characterized by mild interstitial edema and desquamation of rare epithelial cells; 2 = mild, characterized by interstitial edema, thickening of alveolar walls, and occasional bronchial structural damage; 3 = moderate, characterized by hyperemia, hemorrhage, interstitial edema, thickening of the alveolar wall, bronchial structural damage, and slight infiltration of inflammatory cells; and 4 = severe, characterized by hyperemia, hemorrhage, interstitial edema, thickening of the alveolar wall, serious bronchial structural damage, and greater infiltration of inflammatory cells. Detection of the IAV antigen was scored as 0–4. Scoring was based on the number of positive cells per section. Descriptions of the scores are as follows: 0 = no positive cells; 1 = 1–10 positive cells; 2 = 11–30 positive cells; 3 = 31–100 positive cells; and 4 > 100 positive cells.

Quantitative PCR (qPCR) and Enzyme-Linked Immunosorbent Assay (ELISA)

QPCR and ELISA analyses were conducted as previously described.³⁸ Briefly, total RNA was extracted from approximately 10 mg of lung or spleen tissue homogenized in TRIzol reagent (Invitrogen, Carlsbad, CA, USA) and cDNA was reverse transcribed using the EasyScript First-Strand cDNA Synthesis Super Mix (TransGen Biotech, Beijing, China) according to the manufacturer's instructions. Real-time PCR was performed in triplicate using the Power SYBR® Green PCR Master Mix kit (Applied Biosystems,

Warrington, UK) on an Applied Biosystems 7500 system. Expression of the hemagglutinin (HA) gene was measured using the absolute quantification method. Amplification was performed as follows: 10 min at 95°C, followed by 40 cycles of 95°C for 15 s, 50°C for 30 s, and 72°C for 30 s. The copy number was calculated using an HA-containing plasmid of known concentration as a standard. The expression levels of interferon (IFN)- α , IFN- β , IFN- γ , monocyte chemoattractant protein (MCP)-1, interleukin (IL)-1 β , IL-6, IL-12, interferon-induced protein (IP)-10, and tumor necrosis factor (TNF)- α were measured using the relative quantification method, and normalized to the results of the control or glucose group using the $2^{-\Delta\Delta CT}$ method with β -actin (forward primer, 5'-GAG ACC TTC AAC ACC CCG C-3'; reverse primer, 5'-ATG TCA CGC ACG ATT TCC C-3') as an internal standard. Amplification was performed as follows: 10 min at 95°C, followed by 40 cycles of 95°C for 15 s, 50°C for 30 s, and 72°C for 40 s. Cytokine primers are listed in [Table S2](#). In addition, detection of protein expression of cytokines was performed using ELISA kits according to the manufacturer's instructions.

Plaque Assay

Madin–Darby canine kidney (MDCK) cells were cultured in Dulbecco's modified Eagle medium (DMEM) (HyClone Laboratories, Logan, UT, USA) containing 10% fetal bovine serum (HyClone Laboratories), 100 U/mL penicillin, and 100 μ g/mL streptomycin. Right lung homogenates from individual mice were prepared and diluted 10-fold in DMEM and added to a monolayer of MDCK cells in semisolid agar containing 0.5 μ g/mL trypsin-tolylsulfonyl phenylalanyl chloromethyl ketone (TPCK) (Sigma, Beijing, China). The cultures were incubated at 37°C and 5% CO₂ for 60–72 h, fixed, and stained with 1% crystal violet. Plaque-forming units (PFUs) were then counted.

Dendritic Cell (DC) Surface Staining for Co-Stimulatory Molecules

Fluorescent conjugated rat anti-mouse monoclonal antibodies including anti-CD40-PE, anti-CD80-PE, anti-CD86-PE, anti-MHC-II-PE, and anti-CD11c-FITC were purchased from eBiosciences (San Diego, CA, USA). Three non-infected mice from each group were sacrificed on day 1 and another three on day 3 following intraperitoneal administration, and single-cell suspensions were isolated from their spleens. Stimulated cells were fixed with 4% paraformaldehyde and permeabilized with 0.1% saponin (Sigma-

Aldrich) for complete intracellular staining. Cells were then double-stained with antibodies for 30 min at 4°C. The fluorescence intensities were measured with the FACSVerse system and analyzed with FlowJo software (BD Biosciences, San Jose, CA, USA).

Statistical Analysis

Statistical analysis was performed using two-way analysis of variance with the GraphPad Prism (version 5.0; GraphPad Software, San Diego, CA, USA) software package. P-values < 0.05 were considered representative of statistically significant differences.

Results

ZrO₂ Increased Survival of H5N1-Infected Mice

To study the protective effects of NPs in IAV H5N1 infection in vivo, three kinds of NPs, namely ZrO₂, SNs, and PS, were administrated twice intraperitoneally to mice at 100 mg/kg, one day apart. These NPs were prepared according to previous studies. All three sizes (100, 150, and 200 nm) of ZrO₂ showed good monodispersity in 5% glucose solution ([Figure 1](#)). Particles of approximately 100, 150, and 200 nm diameters were observed using transmission electron microscopy. [Table S1](#) showed the hydrodynamic diameter of these particles characterized using the Zetasizer 3000HSA. The NPs were modified with polyethylene glycol, carboxyl, and amidogen to obtain particles with similar positive or neutral surface charges.

NPs were administered to mice intraperitoneally in two doses, one day apart. On the day of the second NP administration, the viral challenge was given with triple LD50 of H5N1, and seven mice per group were used in the experiment over a period of 14 days. As shown in [Figure 2A](#) and [Figure S1A](#), ZrO₂, SNs, and PS of different diameters (100, 150, and 200 nm) were administered. Four mice died in the glucose group; one animal died in each of the 200 nm SN and ZrO₂ treatment groups, and no deaths were observed in the 200 nm PS treatment group. According to the size effect, the survival rate of mice in the 200 nm ZrO₂ group was 85.7%, which was significantly higher than that in the glucose group (42.9%), 100 nm ZrO₂ group (57.1%), or 150 nm ZrO₂ group (42.9%). Moreover, the average body weight of mice treated with NPs at 200 nm was higher than those of other groups throughout the experimental period. The results thus indicate that NPs provide protection

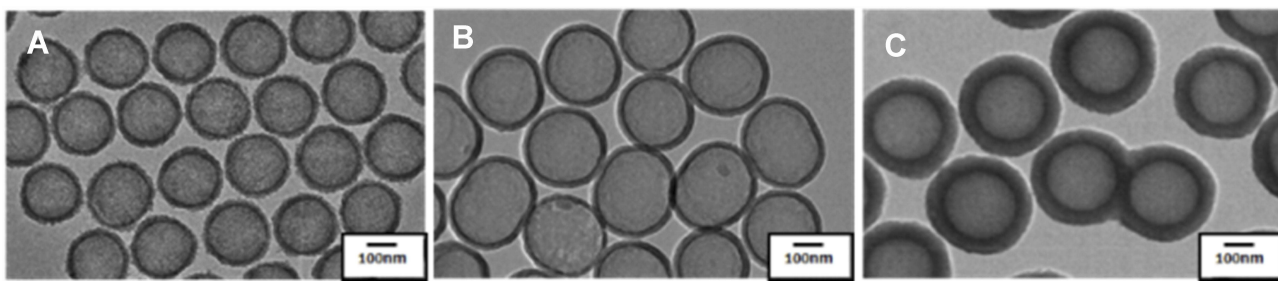


Figure 1 Transmission electron microscopy images of various diameters of ZrO_2 in 5% glucose solution. The well-defined size and shape of 100 (**A**), 100 (**B**), and 200 nm (**C**) ZrO_2 nanoparticles (NPs) allowed for good monodispersity in 5% glucose solution. The scale bar is 100 nm.

against H5N1 that is particle-size-dependent, and the best protection is offered by the 200 nm particle size.

The effect of surface charges of NPs on their antiviral efficacy was studied using 200 nm NPs with positive and negative charges. ZrO_2 , SNs, and PS NPs with both charges were administered to H5N1-infected mice at 100 mg/kg. As shown in [Figure 2B](#) and [Figure S1B](#), compared to the glucose group, in which 4 of 7 mice died, only one mouse died in the group treated with positive NPs. The survival rate of mice in the glucose group was 42.9%, while the P- ZrO_2 and N- ZrO_2 groups had survival rates of 85.7% and 57.1%, respectively. No significant differences were found between glucose and negatively-charged NPs in terms of death rate. These results show that positively-charged NPs confer a higher survival rate and constant body weight, thereby providing enhanced protection against H5N1. Numerous studies have discussed the relationship between NP physicochemical properties and their biological effects.^{39,40} Some reports have shown that particle size plays an important role in the biological effects of NPs, including cellular uptake and toxicity.⁴¹ Size plays a key role in the physiological response, bio-distribution, and elimination of various materials.⁴² Furthermore, surface modification of NPs is critical, as it may lead to altered cellular uptake and endosomal escape of NPs. Lin et al reported that particle uptake by cells increased following the same trend as their surface charges.⁴³ The results of the present study suggest that positively-charged NPs of the appropriate size have a stronger antiviral effect against H5N1 compared to negatively-charged NPs.

To explore whether the effect of NPs against H5N1 infection was dose-dependent, an experiment was performed using ZrO_2 , SNs, and PS at different dosages. We found that NPs could dramatically increase the survival rate and reduce the average body weight of mice

within a narrower range compared to the glucose group. The survival rates of mice in the 25 mg/kg ZrO_2 , 50 mg/kg ZrO_2 , and 100 mg/kg ZrO_2 groups were 100%, 85.7%, and 100%, which were all significantly higher than that in the glucose group (42.9%). Although the survival rates showed modest differences among dosages of NPs, the range of weight loss was reduced with increasing dosage ([Figure 2C](#) and [Figure S1C](#)). Together, these results suggest that 200 nm positively-charged ZrO_2 at a dosage of 100 mg/kg could improve the survival of H5N1-infected mice.

ZrO₂ Reduced Lung Injury and Viral Replication in H5N1-Infected Mice

To further investigate whether ZrO_2 could affect H5N1 virus infection, BALB/c mice received a dose of triple the LD50 of H5N1 on the second day of NP administration via intraperitoneal injection. On days 3 and 6 post-infection, lung tissue samples from three mice per group were collected for histopathological analysis and real-time PCR. As shown in [Figure 3A](#), we examined histopathological changes in the lungs of mice on day 6. Lung lesions in the glucose group included inflammatory cellular infiltration, necrosis of the mucous epithelium of bronchioles, and interstitial edema. Thickening of alveolar walls and alveolar lumen filled with edema fluid mixed with exfoliated alveolar epithelial cells, erythrocytes, and inflammatory cells was also observed in the control group. However, these symptoms appeared to be mitigated in the ZrO_2 groups. Similar symptoms to those observed in the glucose group were seen in the 25 mg/kg ZrO_2 group, but the lesion severity was lower. Both the 50 mg/kg ZrO_2 and 100 mg/kg ZrO_2 groups showed only interstitial edema; in the surrounding lung tissue, inflammatory cell infiltration was observed in the small blood vessels and bronchi. The lung tissues from mice in the

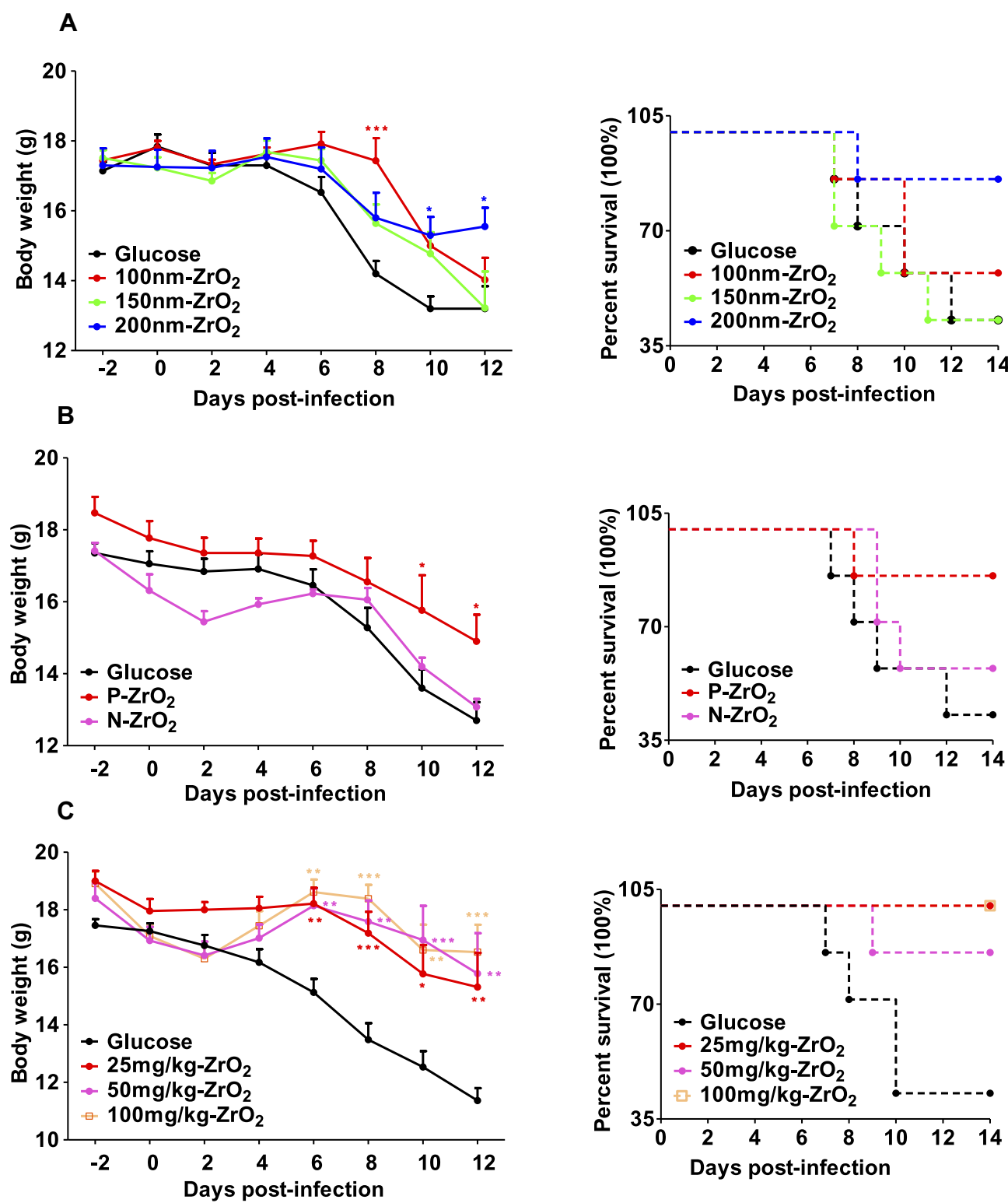


Figure 2 Positively-charged ZrO₂ at a dosage of 100 mg/kg increased survival of H5NI-infected mice. ZrO₂ of different diameters (100, 150, and 200 nm) (**A**), with different charges (positive and negative) (**B**) or at different dosages (25, 50, and 100 mg/kg) (**C**) were administered twice intraperitoneally to mice, one day apart. On the second day of NP administration, the viral challenge was administered, with triple the LD50 of H5NI. Body weights were determined every 2 days. *, P < 0.05; **, P < 0.01; ***, P < 0.001 and compared to the glucose group.

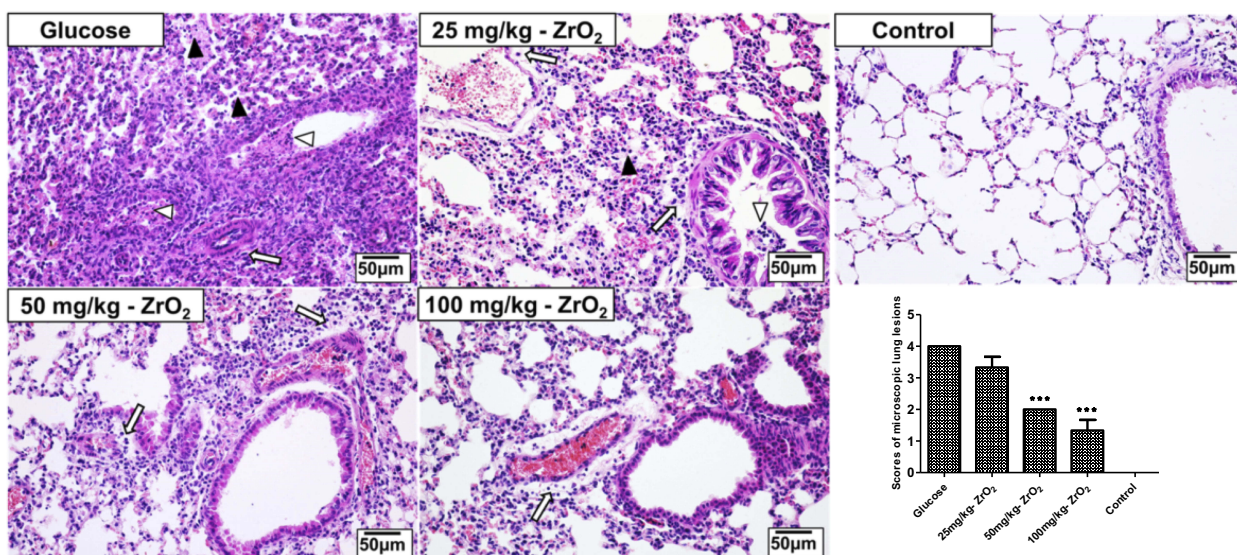
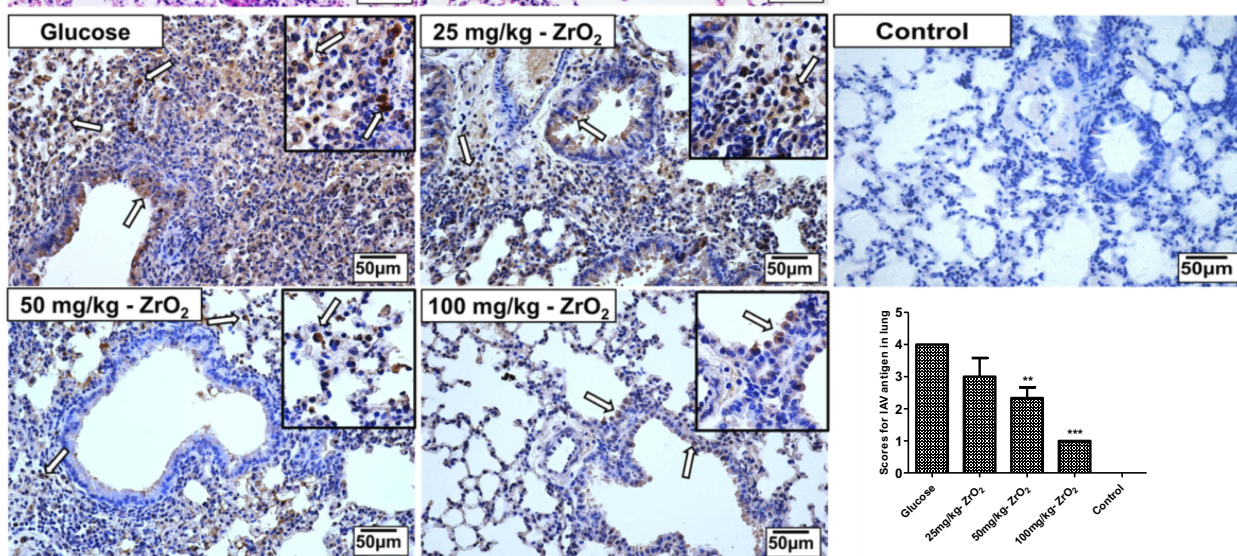
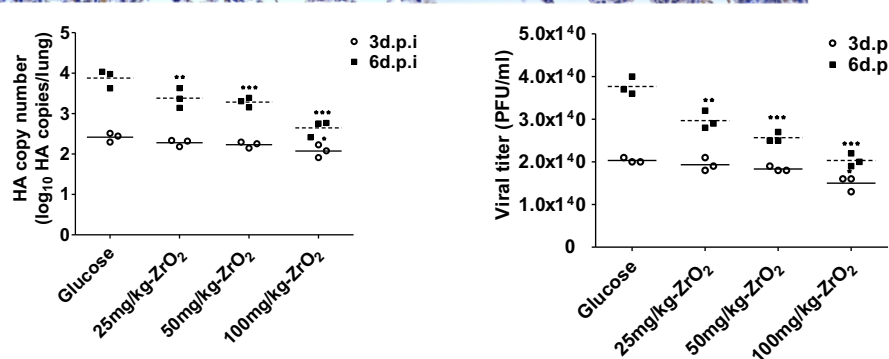
A**B****C**

Figure 3 Positively-charged ZrO₂ NPs of 200 nm reduced lung injury and viral replication in H5N1-infected mice. **(A)** Representative lung sections from each group were stained with H&E (400×) and scored in a blind study. The black triangles show alveolar lumen flooded with edema fluid and mixed with exfoliated alveolar epithelial cells, inflammatory cells, and erythrocytes. Arrows represent interstitial edema and inflammatory cellular infiltration around small blood vessels and bronchioles. Empty triangles indicate reduction in the number of mucous epithelial cells in bronchioles. **(B)** Representative lung sections from each group were stained using IHC (400×) and scored in a blind study. Arrows indicate positive cells. **(C)** Expression levels of HA genes were determined via qPCR and their PFU values were determined through plaque assay. These results were obtained from three distinct animals and are representative of three independent experiments. *, P < 0.05; **, P < 0.01 and ***, P < 0.001 compared to the glucose group.

100 mg/kg ZrO₂ group showed markedly milder symptoms than those from other groups. The control group showed no histopathological changes. The scores of pathological changes in lungs of the H5N1-infected mice were determined. The results suggested that NPs could alleviate lung lesions in H5N1-infected mice.

In the glucose group, IAV antigen was observed in mucosal epithelium cells, deciduous alveolar cells, and the lamina propria of bronchioles in the lungs of mice through IHC analysis, while the presence of antigens in the ZrO₂ groups was sporadic (Figure 3B). In the 25 mg/kg ZrO₂ and 50 mg/kg ZrO₂ groups, low levels of positive signals were observed in alveolar cells and

the lamina propria of bronchioles. Furthermore, few positive signals, which were only distributed in the lamina propria of bronchioles, were detected in the 100 mg/kg ZrO₂ group. No positive cells were observed in the control group. The scores of IAV antigens in the lungs of H5N1-infected mice were determined. To investigate the influence of ZrO₂ on replication of IAV in vivo, the viral load in the lung tissues of virus-infected mice was examined. As shown in Figure 3C, HA copy numbers and PFU values in the ZrO₂ groups at day 6 post-infection were lower than those of glucose-treated mice, with the 100 mg/kg ZrO₂ group showing a significant difference ($P < 0.05$). At day 6

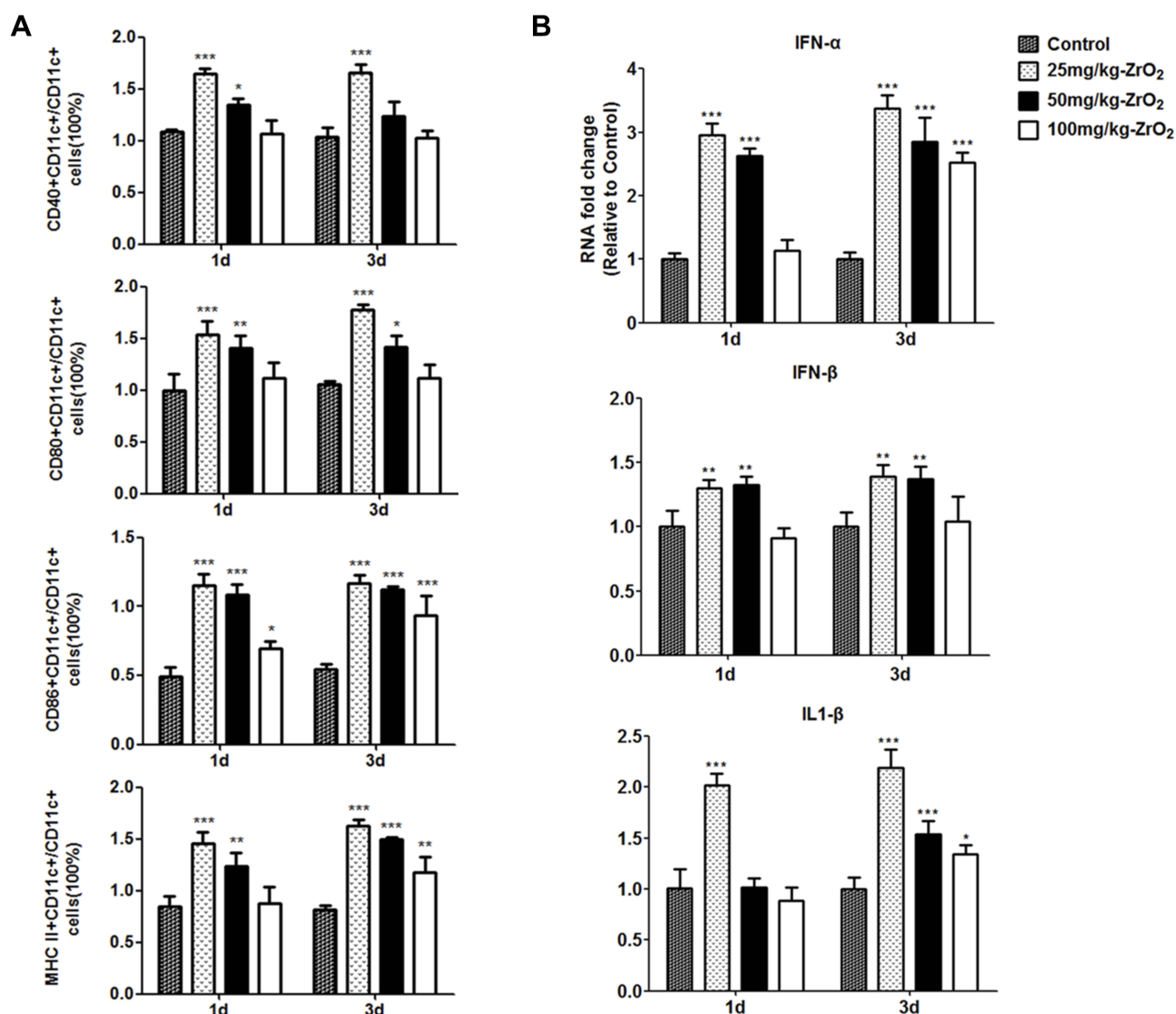


Figure 4 Positively-charged ZrO₂ NPs of 200 nm could enhance the maturation of dendritic cells (DCs) and promote expression of cytokines associated with innate immunity in mice. Non-infected mice were sacrificed on days 1 and 3 after intraperitoneal administration and spleens were collected. (A) Maturation of DCs was measured through FACS analysis. (B) Expression levels of cytokines (IFN- α , IFN- β , and IL1- β) were determined through qPCR. These results are mean \pm SD values obtained from three distinct animals and are representative of three independent experiments. *, $P < 0.05$; **, $P < 0.01$; and ***, $P < 0.001$ compared to the control group.

post-infection, the pulmonary viral titers of ZrO₂ groups were significantly lower than those of glucose-treated mice, with extremely significant differences found for both the 50 mg/kg ZrO₂ and 100 mg/kg ZrO₂ groups ($P < 0.001$). These viral titer results were in accordance with the results of IHC staining. Taken together, ZrO₂ reduces lung injury and viral replication in H5N1-infected mice.

ZrO₂ Enhanced the Innate Immunity of Mice

The activation or maturation of DCs is critical for both innate and adaptive immunity. During initiation of the immune response, the expression of co-stimulatory markers CD40, CD80, and CD86 at the DC surface is related to their ability to induce or suppress immune responses, as is MHC-II expression. Thus, the proportions of CD40+ CD11c+, CD80+ CD11c+, CD86+ CD11c+, and MHC-II+ CD11c+ cells among mouse T cells on days 1 and 3 after intraperitoneal ZrO₂ administration were determined using fluorescence-activated cell sorting (FACS; Figure 4A). CD40, CD80, CD86, and MHC-II expression levels in the ZrO₂ groups were higher than those of the control group, with a significant difference between the 25 mg/kg ZrO₂ and glucose groups ($P < 0.001$). Notably, we found that the higher dosage of ZrO₂ resulted in lower expression, which was due to toxicity of ZrO₂ in normal mice. These data suggest that 200 nm ZrO₂ can promote CD40, CD80, CD86, and MHC-II expression in T cells of mice and favorably affect the maturation of DCs.

IFN- α , IFN- β , and IL1- β are crucial for the innate immune and antiviral responses. To examine the effects of ZrO₂ on cytokine expression in mice, the mRNA levels of IFN- α , IFN- β , and IL1- β in the spleens of mice on days 1 and 3 after intraperitoneal administration were examined. The mRNA levels of the ZrO₂ groups were upregulated compared to the glucose group. With 25 mg/kg ZrO₂ treatment, the expression levels of all cytokines increased significantly. The mRNA levels in the 100 mg/kg ZrO₂ group were lowest among the three ZrO₂ groups due to the toxicity of ZrO₂ in mice (Figure 4B). Furthermore, the mRNA expression profiles of all cytokines in each ZrO₂ group on day 3 after intraperitoneal administration were higher than those on day 1. These data suggested that ZrO₂ promotes the expression of cytokines associated with the antiviral response and innate immunity. Consistent with the FACS results, we found that ZrO₂ effectively enhances innate immunity in mice.

ZrO₂ Reduces the Overexpression of Inflammatory Cytokines in H5N1-Infected Mice

For mechanistic analysis, we evaluated expression levels of the cytokines IFN- γ , IP-10, MCP-1, IL-12, IL-6, and TNF- α in the lungs of infected mice administered NPs using qPCR (Figure 5A). Compared with the glucose group, the mRNA levels of mice in the ZrO₂ group were reduced, and those in the 100 mg/kg ZrO₂ group showed significantly lower expression levels ($P < 0.05$). Combined with histopathological analyses and the detection of HA copy numbers, these results confirm that NPs can alleviate pathological injury and reduce viral levels in the lungs through degradation of the cytokine storm. The cytokine storm occurs when excessive levels of pro-inflammatory cytokines induce an acute mononuclear and neutrophilic inflammatory response.⁴⁴ ELISA results also showed significantly lower protein expression levels of cytokines in the 100 mg/kg ZrO₂ group compared with the other groups at 6 days post-infection, consistent with the results of qPCR (Figure 5B). In the present study, we found that positively-charged ZrO₂ at 200 nm can reduce the production of cytokines involved in the cytokine storm and consequently protect animals from viral infection.

Discussions

Influenza A virus is one of the most common respiratory pathogens worldwide. In 1997, the first major epidemic of highly pathogenic avian influenza virus H5N1 occurred in Hong Kong. Since then, it has become well known for its potential to cause global pandemics in humans and mammals at all ages with considerable risks of morbidity and high fatality rates; it is now considered a growing threat to public health around the world.^{45,46} To date, it has been classified as a List A disease by the World Organisation for Animal Health (OIE) and as a Category 1 animal disease in China. A variety of antiviral drugs and vaccines have been adopted to prevent and control influenza-induced illness. However, it remains difficult to limit the spread of these viruses due to their highly contagious nature, frequent mutation of viral genes, and the emergence of resistant influenza strains due to the widespread abuse of antiviral drugs. Therefore, new approaches to fighting influenza virus infection are urgently needed. Due to unique structure and chemical characteristics, including large surface area, strong targeting performance, good biocompatibility, and high adsorption capacity, NPs

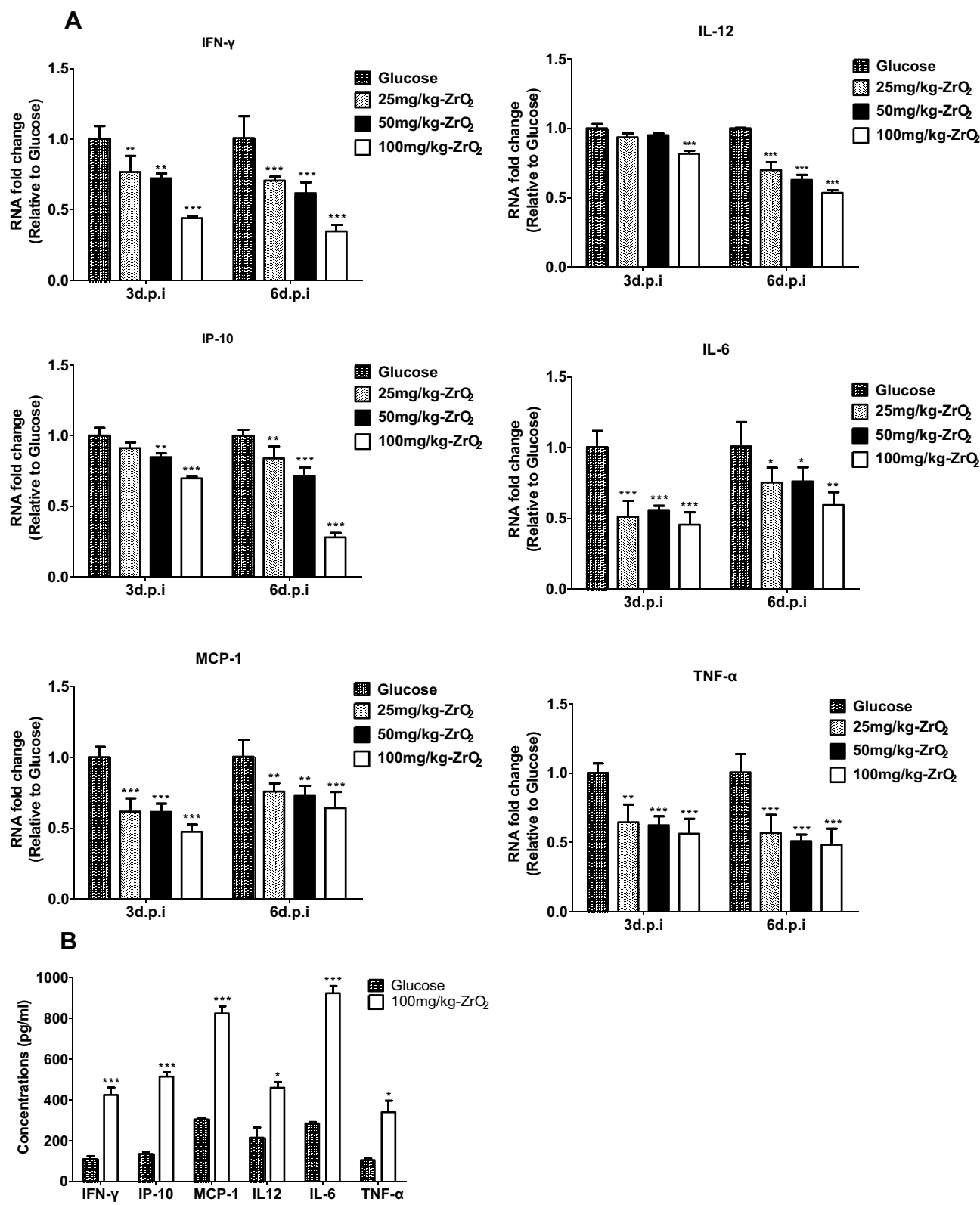


Figure 5 Positively-charged ZrO₂ NPs of 200 nm suppressed cytokine overexpression in the lungs of H5N1-infected mice. The expression levels of cytokines (IFN- γ , IP-10, MCP-1, IL-12, IL-6, and TNF- α) in the lung were determined through qPCR (A) and ELISA (B). These results are mean \pm SD values obtained from three distinct animals and are representative of three independent experiments. *, P < 0.05; **, P < 0.01; and ***, P < 0.001 compared to the glucose group.

have many benefits over conventional materials. Therefore, NPs have been widely applied in clinical trials. As carriers of anti-tumor drugs, NPs can significantly improve the curative effects of tumor therapies and reduce toxic drug side effects, making them attractive candidates for cancer therapy.^{47,48} For anti-viral therapy, NPs can be used as adjuvants or carriers to enhance the immune response.⁴⁹ However, while NPs are commonly used as efficient antigen delivery systems, their antiviral effects have only been recently reported. Herein, we have demonstrated that NPs alone effectively inhibit viral replication in a mouse model and protect mice from H5N1 infection. Our data further confirm the feasibility of the use of NPs alone as therapeutic agents to control influenza infection.

H5N1 influenza virus can cause severe respiratory diseases in humans and mammals. The clinical symptoms include fever, muscle aches, cough, headache, diarrhea,

viral pneumonia, encephalitis, and acute respiratory distress syndrome (ARDS).⁵⁰ In the mouse model, it can cause hair thickening, bowed limbs, blindness, trembling, significant weight loss, severe pathological tissue changes, and even death.⁵¹ Previous studies have shown that virus-induced acute lung injury or ARDS is triggered by a cytokine storm and is a serious consequence of inflammation resulting from the release of pro-inflammatory cytokines and the recruitment of immune cells to the infected area.⁵² Excessive inflammation can cause systemic inflammatory response syndrome, during which the body enters a state of high metabolic activity and energy usage. High levels of pro-inflammatory cytokines, including IL-6, IFN- γ , MCP-1, and TNF- α , have been detected in humans and mice infected with highly pathogenic H5N1 influenza virus.^{53,54} In the present study, we investigated the antiviral effects of positively-charged ZrO₂ on IAV in

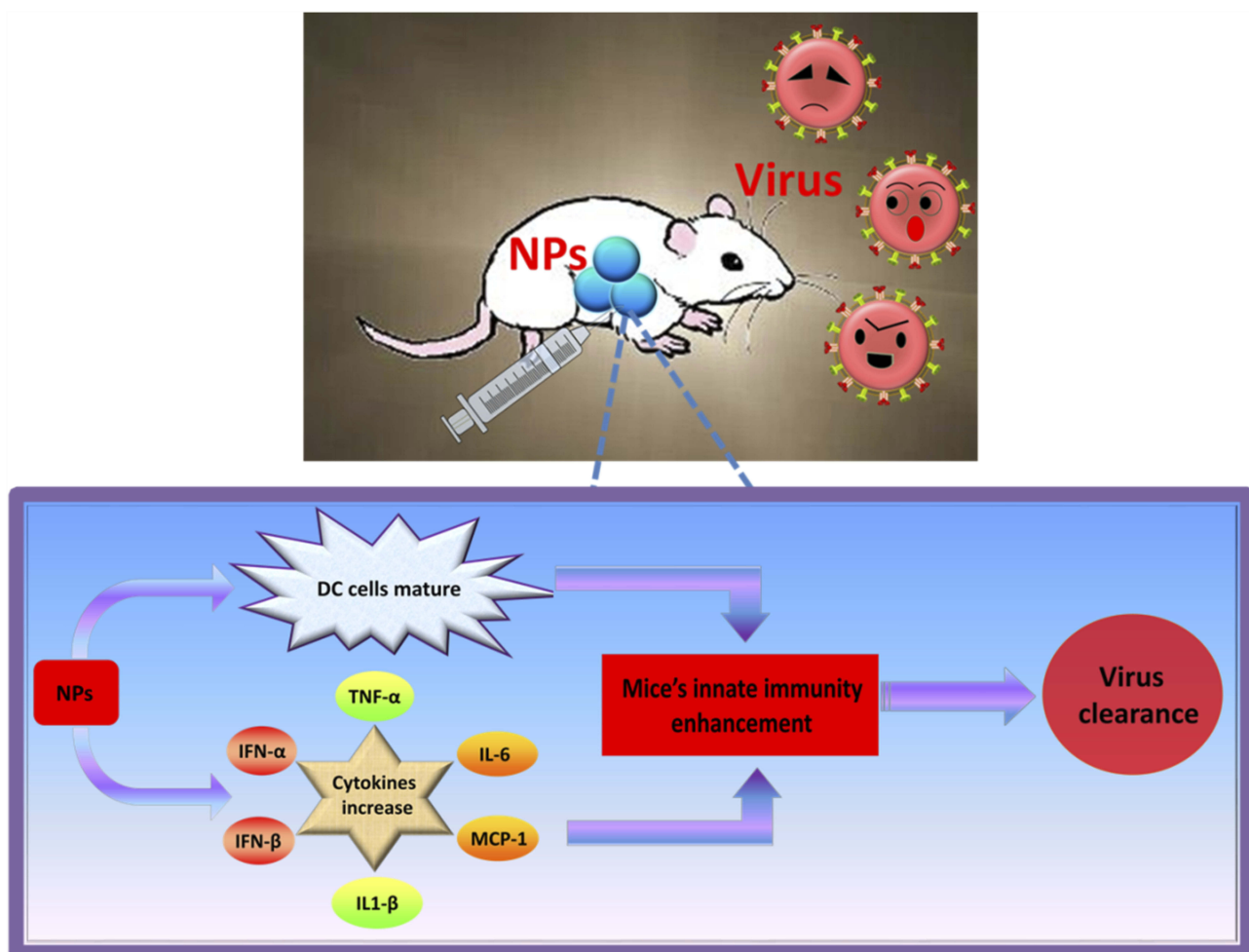


Figure 6 Overview of findings. Positively-charged ZrO₂ of 200 nm size and 100 mg/kg dose conferred protection against H5N1 infection in mice. The mechanisms are related to ZrO₂-mediated enhancement of innate immunity in the early stage of H5N1 infection. The appropriate nanoparticle treatment could reduce viral load and suppress the inflammatory cytokine storm in the lungs of H5N1-infected mice, thus preventing lung injury and improving the survival rate of the infected mice.

a mouse model and the mechanism of action of these NPs. Several studies have shown that positive charges can facilitate retention of NPs in cells for a relatively long time, which is likely related to intracellular agglomeration. The native surface chemistries of NPs also play crucial roles in their exocytosis patterns from cells. Here, we provide the first data that positively-charged ZrO₂ NPs can downregulate the levels of pro-inflammatory cytokines and thereby alleviate the inflammatory response, making them effective anti-inflammatory agents against highly pathogenic H5N1 influenza virus.

In the present study, it seems paradoxical that 100 mg/kg ZrO₂ NPs is less effective for activation of DCs but appears to be more effective in protection when compared to lower doses. Previous researches by our team have researched the systemic toxicity of ZrO₂ NPs and demonstrated that dosages of ZrO₂ in the range of 100–350 mg/kg are safe for effectively clinical use.³³ However, we found that 100 mg/kg ZrO₂ NPs seemed to have a mild adverse reaction in H5N1-infected mice, which only showed the slightly low spirits just on day 1 after intraperitoneal administration. Thus, we consider that this clinical phenomenon may lead to the lower expression of immune indicators in spleen of the 100 mg/kg ZrO₂ group. Compared to 25 mg/kg ZrO₂ NPs or 50 mg/kg ZrO₂ NPs, 100 mg/kg ZrO₂ NPs group showed the most dramatic increases with time increasing, indicating its growing powerful immune responses. We suppose that 100 mg/kg ZrO₂ NPs group will show the better immune responses on day 7 or day 9 after intraperitoneal administration, which will be further investigated in future studies. Due to that NPs could be carried into the lung through the circulation, we speculate that 100 mg/kg ZrO₂ NPs can be carried into lung most effectively after viral infection when compared to 25 mg/kg ZrO₂ NPs and 50 mg/kg ZrO₂ NPs, and then 100 mg/kg ZrO₂ NPs activate the antiviral responses in lung and eventually provide best protection for mice to fight against virus.

Conclusions

We demonstrated that positively-charged ZrO₂ of 200 nm size and 100 mg/kg dose conferred protection against H5N1 infection in mice (Figure 6). The mechanisms of this protection are related to ZrO₂-mediated enhancement of innate immunity in the early stage of H5N1 infection. Appropriate NP treatment could reduce the viral load and suppress the inflammatory cytokine storm in the lungs of H5N1-infected mice, thus alleviating lung injury and improving the survival rate of infected mice. Our antiviral

study using zirconia NPs suggests strong potential for application of this novel treatment to a wide range of microbial infections.

Highlights

- ZrO₂NPs effectively protected mice against the highly pathogenic H5N1 infection.
- ZrO₂ NPs enhance innate immunity and promote cytokines releasing in mice.
- ZrO₂ NPs improve the survival rate of H5N1-infected mice and alleviate lung injury.
- ZrO₂ NPs reduce the viral load and suppress the inflammatory storm in H5N1- infected mice.

Data Sharing Statement

All data generated or analyzed during this study are included in this published article.

Acknowledgments

The authors acknowledge financial supports from the National Natural Science Foundation of China (Grant no. 31772702), the Chinese Universities Scientific Fund (Grant no. 2018TC044) and the National Twelve-five Technological Supported Plan of China (Grant no: 2015BAD12B01). The English in this document has been checked by at least two professional editors, both native speakers of English.

Author Contributions

All authors contributed to data analysis, drafting or revising the article, gave final approval of the version to be published, and agree to be accountable for all aspects of the work.

Disclosure

The authors report no conflicts of interest in this work.

References

1. Werneck LMC, Vieira CB, Fumian TM, et al. Dissemination of gastroenteric viruses in the production of lettuce in developing countries: a public health concern. *FEMS Microbiol Lett*. 2017;364(9). doi:10.1093/femsle/fnx085
2. Brito BP, Rodriguez LL, Hammond JM, Pinto J, Perez AM. Review of the global distribution of foot-and-mouth disease virus from 2007 to 2014. *Transbound Emerg Dis*. 2017;64(2):316–332. doi:10.1111/tbed.2017.64.issue-2
3. Meng B, Wang J, Liu J, Wu J, Zhong E. Understanding the spatial diffusion process of severe acute respiratory syndrome in Beijing. *Public Health*. 2005;119(12):1080–1087. doi:10.1016/j.puhe.2005.02.003

4. Thomas M, Mani RS, Philip M, et al. Proinflammatory chemokines are major mediators of exuberant immune response associated with Influenza A (H1N1) pdm09 virus infection. *J Med Virol.* **2017**;89(8):1373–1381. doi:10.1002/jmv.24781
5. Yu Y, Zhang Z, Li H, et al. Biological characterizations of H5Nx avian influenza viruses embodying different neuraminidases. *Front Microbiol.* **2017**;8:1084. doi:10.3389/fmicb.2017.01084
6. Gonzales JL, Elbers AR, Bouma A, Koch G, de Wit JJ, Stegeman JA. Transmission characteristics of low pathogenic avian influenza virus of H7N7 and H5N7 subtypes in layer chickens. *Vet Microbiol.* **2012**;155(2–4):207–213. doi:10.1016/j.vetmic.2011.09.016
7. Noh JY, Yoon SW, Kim DJ, et al. Simultaneous detection of severe acute respiratory syndrome, Middle East respiratory syndrome, and related bat coronaviruses by real-time reverse transcription PCR. *Arch Virol.* **2017**;162(6):1617–1623. doi:10.1007/s00705-017-3281-9
8. Zhu FC, Wurie AH, Hou LH, et al. Safety and immunogenicity of a recombinant adenovirus type-5 vector-based Ebola vaccine in healthy adults in Sierra Leone: a single-centre, randomised, double-blind, placebo-controlled, Phase 2 trial. *Lancet.* **2017**;389(10069):621–628. doi:10.1016/S0140-6736(16)32617-4
9. Brooks T, Roy-Burman A, Tuholcs C, et al. Real-time evolution of zika virus disease outbreak, Roatan, Honduras. *Emerg Infect Dis.* **2017**;23(8). doi:10.3201/eid2308.161944
10. Marinova-Petkova A, Franks J, Tenzin S, et al. Highly pathogenic reassortant avian influenza A(H5N1) Virus Clade 2.3.2.1a in Poultry, Bhutan. *Emerg Infect Dis.* **2016**;22(12):2137–2141. doi:10.3201/eid2212.160611
11. Ly S, Vong S, Cavailler P, et al. Environmental contamination and risk factors for transmission of highly pathogenic avian influenza A (H5N1) to humans, Cambodia, 2006–2010. *BMC Infect Dis.* **2016**;16(1):631. doi:10.1186/s12879-016-1950-z
12. Zhang Z, Li R, Jiang L, et al. The complexity of human infected AIV H5N6 isolated from China. *BMC Infect Dis.* **2016**;16(1):600. doi:10.1186/s12879-016-1932-1
13. Bethmont A, Bui CM, Gardner L, Sarkar S, Chughtai AA, Macintyre CR. Quantified degree of poultry exposure differs for human cases of avian influenza H5N1 and H7N9. *Epidemiol Infect.* **2016**;144(12):2633–2640. doi:10.1017/S0950268816001035
14. Dae Young K, Hye-Jun K, Junhyeok B, Taeseon Y. Examining the probability of the critical mutation of H5N8 by comparing with H7N9 and H5N1 using apriori algorithm and support vector machine. *Int J Comput Theory Eng.* **2015**;7(2):145–148. doi:10.7763/IJCTE.2015.V7.946
15. Burggraaf S, Karpala AJ, Bingham J, et al. H5N1 infection causes rapid mortality and high cytokine levels in chickens compared to ducks. *Virus Res.* **2014**;185:23–31. doi:10.1016/j.virusres.2014.03.012
16. Chen LH, Leder K, Wilson ME. Closing the gap in travel medicine: reframing research questions for a new era. *J Travel Med.* **2017**;24(4). doi:10.1093/jtm/tax001
17. Marjuki H, Mishin VP, Chesnokov AP, et al. Characterization of drug-resistant influenza A(H7N9) variants isolated from an oseltamivir-treated patient in Taiwan. *J Infect Dis.* **2015**;211(2):249–257. doi:10.1093/infdis/jiu447
18. Wu Y, Gao F, Qi J, et al. Resistance to mutant group 2 influenza virus neuraminidases of an oseltamivir-zanamivir hybrid inhibitor. *J Virol.* **2016**;90(23):10693–10700. doi:10.1128/JVI.01703-16
19. Dasargyri A, Kumin CD, Leroux JC. Targeting nanocarriers with anisamide: fact or artifact? *Advanced materials.* **2017**;29(7):1603451.
20. Batmunkh M, Bat-Erdene M, Shapter JG. Phosphorene and phosphorene-based materials - prospects for future applications. *Adv Mat.* **2016**;28(39):8586–8617.
21. Chen W, Zhang S, Yu Y, Zhang H, He Q. Structural-engineering rationales of gold nanoparticles for cancer theranostics. *Adv Mat.* **2016**;28(39):8567–8585. doi:10.1002/adma.201602080
22. Moon JJ, Huang B, Irvine DJ. Engineering nano- and microparticles to tune immunity. *Adv Mat.* **2012**;24(28):3724–3746. doi:10.1002/adma.v24.28
23. Cui J, De Rose R, Best JP, et al. Mechanically tunable, self-adjuvanting nanoengineered polypeptide particles. *Adv Mat.* **2013**;25(25):3468–3472. doi:10.1002/adma.v25.25
24. Xu L, Liu Y, Chen Z, et al. Morphologically virus-like fullerol nanoparticles act as the dual-functional nanoadjuvant for HIV-1 vaccine. *Adv Mat.* **2013**;25(41):5928–5936. doi:10.1002/adma.201300583
25. Schuller VJ, Heidegger S, Sandholzer N, et al. Cellular immunostimulation by CpG-sequence-coated DNA origami structures. *ACS Nano.* **2011**;5(12):9696–9702. doi:10.1021/nn203161y
26. Liu Y, Balachandran YL, Li D, Shao Y, Jiang X. Polyvinylpyrrolidone-poly(ethylene glycol) modified silver nanorods can be a safe, noncarrier adjuvant for HIV vaccine. *ACS Nano.* **2016**;10(3):3589–3596. doi:10.1021/acsnano.5b08025
27. Zhu G, Zhang F, Ni Q, Niu G, Chen X. Efficient nanovaccine delivery in cancer immunotherapy. *ACS Nano.* **2017**;11(3):2387–2392. doi:10.1021/acsnano.7b00978
28. Sun B, Ji Z, Liao YP, et al. Engineering an effective immune adjuvant by designed control of shape and crystallinity of aluminum oxyhydroxide nanoparticles. *ACS Nano.* **2013**;7(12):10834–10849. doi:10.1021/nn404211j
29. Li Y, Cheng H, Li D, Qin Y, Xie Y, Wang S, WO3/CeO2-ZrO2, a promising catalyst for selective catalytic reduction (SCR) of NOx with NH3 in diesel exhaust. *Chem Commun.* **2008**;12:1470–1472. doi:10.1039/b717873e
30. Joo JB, Vu A, Zhang Q, et al. A sulfated ZrO2 hollow nanostructure as an acid catalyst in the dehydration of fructose to 5-hydroxymethylfurfural. *ChemSusChem.* **2013**;6(10):2001–2008. doi:10.1002/cssc.v6.10
31. Mftah A, Alhassan FH, Al-Qubaisi MS, et al. Physicochemical properties, cytotoxicity, and antimicrobial activity of sulphated zirconia nanoparticles. *Int J Nanomedicine.* **2015**;10:765–774. doi:10.2147/IJN.S66058
32. Chen D, Li L, Tang F, Qi S. Facile and scalable synthesis of tailored silica “nanorattle” structures. *Adv Mat.* **2009**;21(37):3804–3807. doi:10.1002/adma.v21:37
33. Yang Y, Bao H, Chai Q, et al. Toxicity, biodistribution and oxidative damage caused by zirconia nanoparticles after intravenous injection. *Int J Nanomedicine.* **2019**;14:5175–5186. doi:10.2147/IJN.S197565
34. Yu C, Liu G, Zuo B, Tang R. A novel gaseous dimethylamine sensor utilizing cataluminescence on zirconia nanoparticles. *Luminescence.* **2009**;24(5):282–289. doi:10.1002/bio.v24.5
35. Lunov O, Syrovets T, Loos C, et al. Differential uptake of functionalized polystyrene nanoparticles by human macrophages and a monocytic cell line. *ACS Nano.* **2011**;5(3):1657–1669. doi:10.1021/nn2000756
36. Hu Y, Jin Y, Han D, et al. Mast cell-induced lung injury in mice infected with H5N1 influenza virus. *J Virol.* **2012**;86(6):3347–3356. doi:10.1128/JVI.06053-11
37. Jin Y, Hu Y, Han D, Wang M. Chronic heat stress weakened the innate immunity and increased the virulence of highly pathogenic avian influenza virus H5N1 in mice. *J Biomed Biotechnol.* **2011**;2011:367846. doi:10.1155/2011/367846
38. Han D, Wei T, Zhang S, et al. The therapeutic effects of sodium cromoglycate against influenza A virus H5N1 in mice. *Influenza Other Respir Viruses.* **2016**;10(1):57–66. doi:10.1111/irv.12334
39. Vlashi E, Kelderhouse LE, Sturgis JE, Low PS. Effect of folate-targeted nanoparticle size on their rates of penetration into solid tumors. *ACS Nano.* **2013**;7(10):8573–8582. doi:10.1021/nn402644g
40. Nagy A, Steinbruck A, Gao J, Doggett N, Hollingsworth JA, Iyer R. Comprehensive analysis of the effects of CdSe quantum dot size, surface charge, and functionalization on primary human lung cells. *ACS Nano.* **2012**;6(6):4748–4762. doi:10.1021/nn204886b

41. Meng H, Xue M, Xia T, et al. Use of size and a copolymer design feature to improve the biodistribution and the enhanced permeability and retention effect of doxorubicin-loaded mesoporous silica nanoparticles in a murine xenograft tumor model. *ACS Nano*. 2011;5(5):4131–4144. doi:10.1021/mn200809t
42. Lu K, Dong S, Petersen EJ, et al. Biological uptake, distribution, and depuration of radio-labeled graphene in adult zebrafish: effects of graphene size and natural organic matter. *ACS Nano*. 2017;11(3):2872–2885. doi:10.1021/acsnano.6b07982
43. Lin D, Cheng Q, Jiang Q, et al. Intracellular cleavable poly(2-dimethylaminoethyl methacrylate) functionalized mesoporous silica nanoparticles for efficient siRNA delivery in vitro and in vivo. *Nanoscale*. 2013;5(10):4291–4301. doi:10.1039/c3nr00294b
44. Liu Q, Zhou YH, Yang ZQ. The cytokine storm of severe influenza and development of immunomodulatory therapy. *Cell Mol Immunol*. 2016;13(1):3–10. doi:10.1038/cmi.2015.74
45. Uyeki TM. Human infection with highly pathogenic avian influenza A (H5N1) virus: review of clinical issues. *Clin Infect Dis*. 2009;49(2):279–290. doi:10.1086/599186
46. Meng D, Huo C, Wang M, et al. Influenza viruses replicate productively in mouse mastocytoma cells (P815) and trigger pro-inflammatory cytokine and chemokine production through TLR3 signaling pathway. *Front Microbiol*. 2016;7:2130.
47. Qiang L, Meng X, Li L, et al. Preparation of magnetic rattle-type silica through a general and facile pre-shell-post-core process for simultaneous cancer imaging and therapy. *Chem Commun*. 2013;49(72):7902–7904. doi:10.1039/c3cc43660h
48. Li L, Tang F, Liu H, et al. In vivo delivery of silica nanorattle encapsulated docetaxel for liver cancer therapy with low toxicity and high efficacy. *ACS Nano*. 2010;4(11):6874–6882. doi:10.1021/nn100918a
49. Adhikary RR, More P, Banerjee R. Smart nanoparticles as targeting platforms for HIV infections. *Nanoscale*. 2015;7(17):7520–7534. doi:10.1039/C5NR01285F
50. Jin Y, Zhang G, Hu Y, et al. Inhibition of highly pathogenic avian H5N1 influenza virus propagation by RNA oligonucleotides targeting the PB2 gene in combination with celecoxib. *J Gene Med*. 2011;13(4):243–249. doi:10.1002/jgm.v13.4
51. Belser JA, Gustin KM, Katz JM, Maines TR, Tumpey TM. Comparison of traditional intranasal and aerosol inhalation inoculation of mice with influenza A viruses. *Virology*. 2015;481:107–112. doi:10.1016/j.virol.2015.02.041
52. de Jong MD, Simmons CP, Thanh TT, et al. Fatal outcome of human influenza A (H5N1) is associated with high viral load and hypercytokinemia. *Nat Med*. 2006;12(10):1203–1207. doi:10.1038/nm1477
53. Cheung CY, Poon LL, Lau AS, et al. Induction of proinflammatory cytokines in human macrophages by influenza A (H5N1) viruses: a mechanism for the unusual severity of human disease? *Lancet*. 2002;360(9348):1831–1837. doi:10.1016/S0140-6736(02)11772-7
54. Szretter KJ, Gangappa S, Lu X, et al. Role of host cytokine responses in the pathogenesis of avian H5N1 influenza viruses in mice. *J Virol*. 2007;81(6):2736–2744. doi:10.1128/JVI.02336-06

International Journal of Nanomedicine

Dovepress

Publish your work in this journal

The International Journal of Nanomedicine is an international, peer-reviewed journal focusing on the application of nanotechnology in diagnostics, therapeutics, and drug delivery systems throughout the biomedical field. This journal is indexed on PubMed Central, MedLine, CAS, SciSearch®, Current Contents®/Clinical Medicine,

Journal Citation Reports/Science Edition, EMBase, Scopus and the Elsevier Bibliographic databases. The manuscript management system is completely online and includes a very quick and fair peer-review system, which is all easy to use. Visit <http://www.dovepress.com/testimonials.php> to read real quotes from published authors.

Submit your manuscript here: <https://www.dovepress.com/international-journal-of-nanomedicine-journal>